

THE IMPRINT OF COSMIC RAY DRIVEN OUTFLOWS ON LYMAN- α SPECTRA

MAX GRONKE¹, PHILIPP GIRICHIDIS², THORSTEN NAAB³, AND STEFANIE WALCH⁴

¹Department of Physics, University of California, Santa Barbara, CA 93106, USA;

²Leibniz-Institut für Astrophysik Potsdam, An der Sternwarte 16, D-14482 Potsdam, Germany;

³Max-Planck-Institut für Astrophysik, Karl-Schwarzschild-Str. 1, D-85741 Garching, Germany; and

⁴I. Physikalisches Institut, Universität zu Köln, Zùlpicher Str. 77, D-50937 Köln, Germany.

Draft from July 23, 2018

Abstract

Recent magneto-hydrodynamic simulations of the star-forming interstellar medium (ISM) with parsec scale resolution indicate that relativistic cosmic rays support the launching of galactic outflows on scales of a few kpc. If these fundamental constituents of the ISM are injected at the sites of supernova (SN) explosions, the outflows are smoother, colder, and denser than the highly structured, hot-phase driven outflows forming, e.g., by thermal SN energy injection alone. In this Letter we present computations of resonant Lyman- α ($\text{Ly}\alpha$) radiation transfer through snapshots of a suite of stratified disk simulations from the SILCC project. For a range of thermal, radiative, and kinetic feedback models only simulations including non-thermal cosmic rays produce $\text{Ly}\alpha$ spectra with enhanced red peaks and strong absorption at line center – similar to observed systems. The absence of cosmic ray feedback leads to spectra incompatible with observations. We attribute this to the smoother neutral gas distribution of cosmic ray supported outflows within a few kpc from the disk midplane.

Subject headings: galaxies: ISM — line: formation — scattering — radiative transfer — cosmic rays
— galaxies: formation

1. INTRODUCTION

Galactic outflows are commonly detected through absorption and emission line studies (Veilleux et al. 2005; Steidel et al. 2010; Tumlinson et al. 2017). A particularly noteworthy emission line is Lyman- α ($\text{Ly}\alpha$), which is due to the first transition of atomic hydrogen. Partridge & Peebles (1967) realized the potential use of this bright emission line to detect star-forming galaxies, and since then thousands of $\text{Ly}\alpha$ emitting galaxies have been found. However, its use in probing the gas kinematics is limited due to the resonant nature of $\text{Ly}\alpha$, which leads to scattering processes and frequency shifts. Thus, the observed spectrum cannot be directly linked to the kinematics of the emitting regions as for optically thinner lines.

The resonant nature of $\text{Ly}\alpha$ is often seen as a major shortcoming but it holds an immense potential since the $\text{Ly}\alpha$ photons sample – in their semi-random walk through the galaxy – the density and kinematic structure of neutral hydrogen (HI), which are difficult to probe otherwise (Neufeld 1990; Eide et al. 2018).

Comparisons of observed with synthetic $\text{Ly}\alpha$ spectra yield that the majority of spectral shapes are consistent with outflows, and are reproducible even with very simplified models (e.g., Gronke 2017). These functioning models have usually a homogeneous geometry such as a slab or a shell – which is somewhat surprising, as observations (Veilleux et al. 2005), analytic considerations (McKee & Ostriker 1977) as well as numerical simulations (e.g., Walch et al. 2015; Kim & Ostriker 2018) show that the interstellar medium (ISM) and its outflows have a multiphase structure.

The hot phase of this medium – one major driver for outflows – is mainly generated by supernovae (SN) ex-

plosions, which dump large amounts of energy into their surroundings (see, e.g., Naab & Ostriker 2017). Recent ISM scale simulations presented in Girichidis et al. (2018) highlight that the inclusion of cosmic rays (CRs), in addition to SN explosions, change the multiphase structure of the outflows. They become smoother and overall denser transporting more $\sim 10^4$ K gas away from the star-forming disk. Here, we investigate the effect of CR driven outflow features on $\text{Ly}\alpha$ observables. We, therefore, use mainly the simulations of Girichidis et al. (2018) (see §2).

2. METHOD

2.1. The SILCC simulations

The simulation setups are described in detail in Walch et al. (2015) and Girichidis et al. (2016b). For the details of the CR implementation we refer to Girichidis et al. (2016a) and Girichidis et al. (2018). In the following we only give a brief summary. The magneto-hydrodynamic (MHD) simulations are carried out using the FLASH code (Fryxell et al. 2000; Dubey et al. 2009)¹. The representative volume of the SN-driven ISM is a stratified box with a size of $0.5 \text{ kpc} \times 0.5 \text{ kpc} \times \pm 5 \text{ kpc}$. The MHD equations are solved using the HLLR3/5 solver (Waagan et al. 2011), which has been extended to include CRs as a relativistic fluid in the advection-diffusion approximation. Gravitational attraction includes the effects of self-gravity using a tree-based method by Wünsch et al. (2018) as well as an external potential to account for the stellar component of the disk. The thermodynamical evolution is coupled to a chemical network based on Glover & Clark (2012) which follows the evolution of hydrogen in the form of H_2 , H, or H^+ . As a dynamical driver we use SNe that explode at a constant

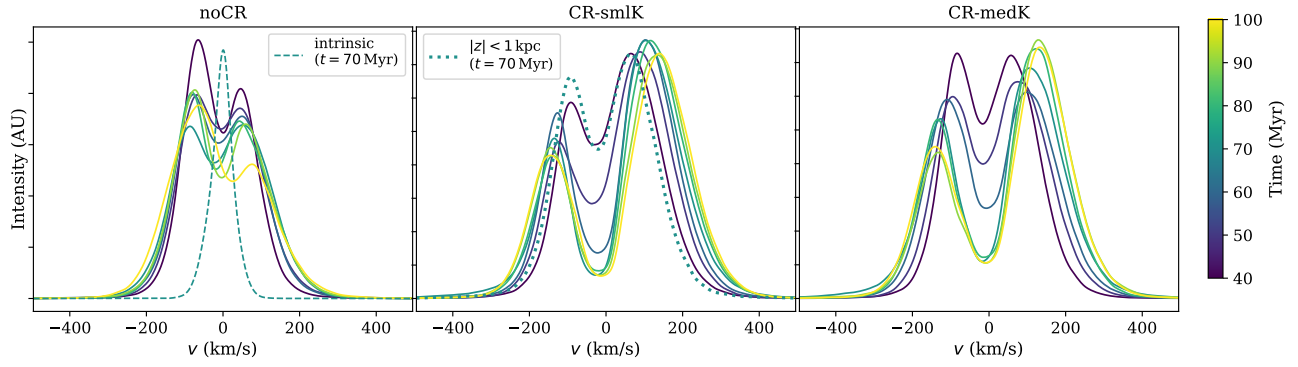


FIG. 1.— Emergent Ly α spectra of the simulations without CRs (*left*) and with CR feedback with small and medium diffusion coefficient (*center and right*). Shown are the spectra from $t = 40$ Myr to $t = 100$ Myr in steps of 10 Myr after the start of the simulation. Only simulations with CRs show the dominant red peak ($v > 0$), and a strong depression at line center at times when the outflow is fully developed ($t \gtrsim 70$ Myr). As examples, the *dashed line* shows an intrinsic spectrum which is widened through radiative transfer effects, and the *dotted line* in shows the spectrum emergent from the inner 1 kpc (both at 70 Myr), i.e., before the photons have to cross the CR driven outflow.

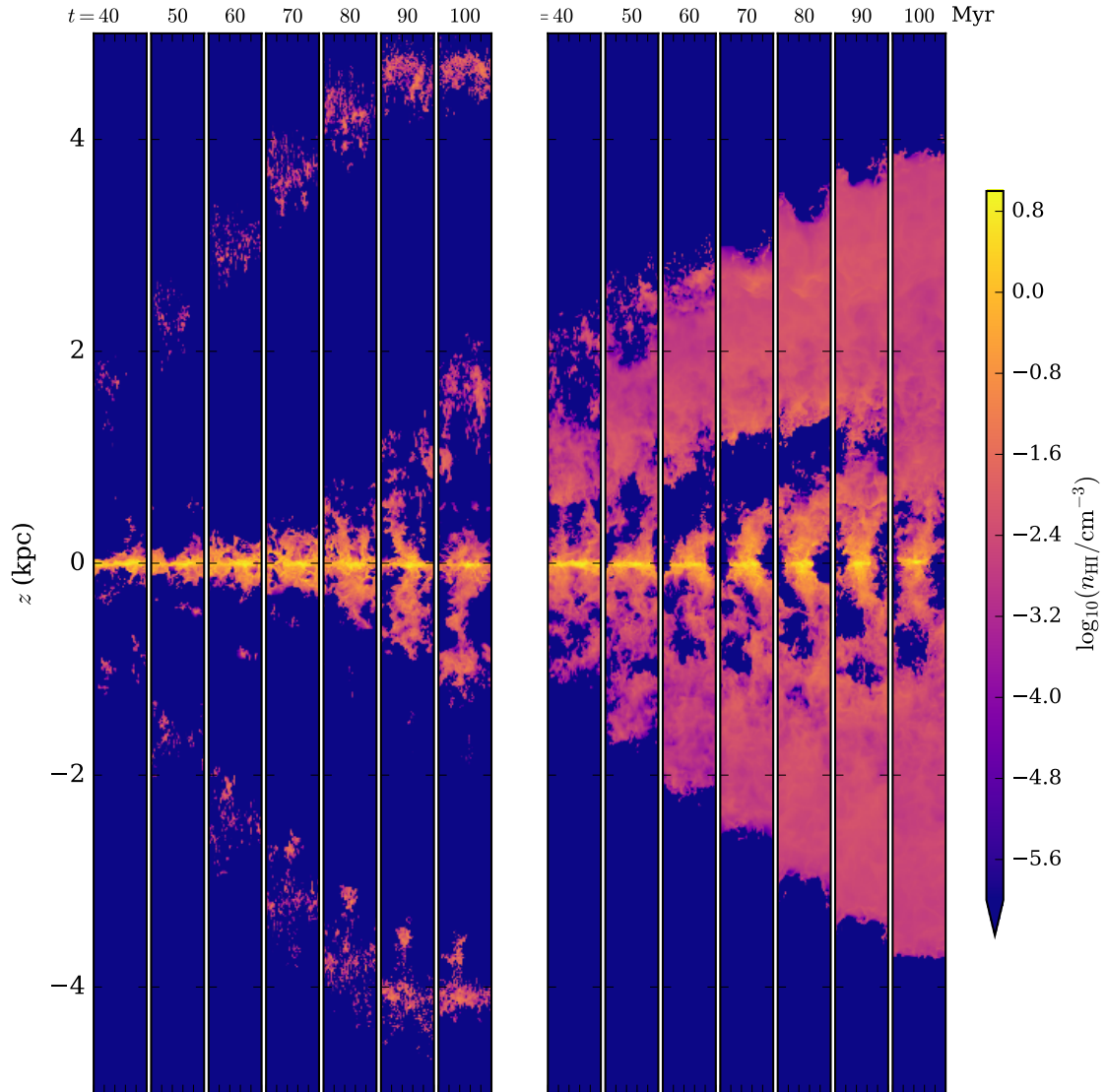


FIG. 2.— Projected n_{HI} distribution of the ‘noCR’ (*left*) and ‘CR-smlK’ simulations (*right*) which shows a smoother and more volume filling HI distribution for the latter. The position of last scattering follows roughly the n_{HI} distribution. Thus, the observable surface brightness distribution would be much more spread out in the ‘CR-smlK’ case.

rate. We consider clustering of the SNe based on observational constraints. For every SN we inject a thermal energy of 10^{51} erg if the Sedov-Taylor radius is resolved with at least 4 cells (which is the case for $\gtrsim 95\%$), otherwise we inject the terminal momentum (see Gatto et al. 2015; Haid et al. 2016). In the case of CRs, we additionally inject 10^{50} erg as CRs. We run the simulations for 100 – 150 Myr.

We mainly use the simulations ‘noCR’, ‘CR-smlK’, and ‘CR-medK’ of Girichidis et al. (2018), which feature no CR feedback, and two different CR diffusion coefficients. For comparison, we also use simulations with a more self-consistent cluster based star formation algorithm and the inclusion of stellar wind (Gatto et al. 2017) and ionizing radiation (Peters et al. 2017).

2.2. Radiative transfer

We use the Monte-Carlo radiative transfer code `tlac` (Gronke & Dijkstra 2014) to follow the trajectories and frequencies of individual photon packages. The emergent spectrum is the distribution of the photons’ frequencies escaping the simulation box (e.g., Dijkstra 2017).

Prior to the radiative transfer calculations, we convert the SILCC output to a uniform grid with cellsize ~ 4 pc, corresponding to the spacing of the maximum refinement of the hydrodynamical simulation. We associate each cell with the following properties:

- the neutral hydrogen number density n_{HI} , which we take directly from the SILCC output,
- the effective temperature T , which is the cell temperature from the hydrodynamical simulation,
- the dust opacity per cell which we calculate following Laursen et al. (2009) as $\kappa_d = \sigma_{\text{SMC}}(n_{\text{HI}} + a_{\text{ion}}n_{\text{HII}})$, where $\sigma_{\text{Ly}\alpha, \text{SMC}} \approx 1.58 \times 10^{-21} \text{ cm}^2$ is the Ly α dust cross section for the Small Magellanic Cloud (Pei 1992), n_{HII} the H^+ number density, and we use a dust-to-gas ratio in the ionized regions of $a_{\text{ion}} = 0.01$,
- the gas bulk velocity \mathbf{v} from the hydrodynamical simulations, and
- the Ly α emissivity $\epsilon = n_{\text{HII}}n_eN_\alpha(T)\alpha_B(T)$ where $N_\alpha(T)$ is the number of Ly α photons produced per recombination event for which we use the fit provided by Cantalupo et al. (2008), and $\alpha_B(T)$ is the ‘case-B’ recombination coefficient as approximated by Hui & Gnedin (1997).

For each photon package we draw the starting position randomly proportional to a cell’s emissivity². The initial frequency is drawn from a Voigt function with mean and width corresponding to the bulk velocity and approximately the thermal velocity of HI, v_{th} , of the starting cell, respectively. A random initial direction (isotropically distributed), and a ‘travelling optical depth’, τ , (from an exponential distribution with unity scale) are drawn. We compute the photon’s travelling distance d

via

$$\tau = \int_0^d ds (n_{\text{HI}}\sigma_{\text{HI}}(v, T) + \kappa_d), \quad (1)$$

where $\sigma_{\text{HI}}(v, T)$ is the Ly α scattering cross section in units of velocity offset from line-center $v = (\nu_{\text{Ly}\alpha}/\nu - 1)c$. Afterwards, the photon scatters off hydrogen with a probability $\sigma_{\text{HI}}n_{\text{HI}}$, or off dust (with a probability $A_d\kappa_d$ where $A_d = 0.32$ is the dust albedo), or is absorbed by dust. After scattering, we draw the new photon direction from the corresponding phase function (see Gronke & Dijkstra 2014).

It is possible to omit the scatterings near line-center leading to essentially no displacement of the photon. We use a (conservative) dynamic core-skipping technique following Smith et al. (2015) with an upper limit $v_{\text{crit.,max}} \sim 10v_{\text{th}}$. We compared some selected spectra to the results obtained for simulations without speeding up the calculations, and found them to be indistinguishable.

3. RESULTS

Fig. 1 shows the computed Ly α spectra for three simulations introduced in Girichidis et al. (2018). In each panel, we show the spectra of the snapshots at $t = 40, 50 \dots 100$ Myr (color-coded) assembled with the photons escaping in the positive z -direction (the Ly α escape fractions are typically $\sim 30 - 80\%$). The escape directions are as for an optically thick slab, i.e., proportional to the cosine of the viewing angle. Each spectrum consists of 10^5 escaped photon packages and was smoothed with a Gaussian kernel (standard deviation $\sigma = 10 \text{ km s}^{-1}$). The left panel shows the results of the ‘noCR’ simulation (only thermal feedback; where we also included as an example an intrinsic spectrum as dashed line) whereas the other two panels show the results of two simulations including CRs. While the spectra of the former simulations stay similar in shape with a fairly symmetric or even dominant blue ($v < 0$) side, the spectra of the CR simulations evolve over time with an increasingly dominant red ($v > 0$) side and a deeper ‘draught’ between the two peaks. The spectra of the ‘downward’ side (photons escaping in a negative z -direction; not shown) look very similar. The ‘noCR’ spectra look quantitatively similar to spectra from similar simulations including self-gravity (Walch et al. 2015; Girichidis et al. 2016b), additional feedback from stellar winds (Gatto et al. 2017), and ionizing radiation (Peters et al. 2017).

This difference in the respective Ly α spectra caused by the CR feedback can be understood when analyzing the morphology of the neutral gas. In Fig. 2 we show the two-dimensional projection of the neutral hydrogen in our simulation boxes with (right) and without CRs (left). Clearly visible in both cases is the dense, central disk extending over $z \lesssim 0.2$ kpc. There is additional neutral gas at larger heights which has been expelled from the inner disk. This gas is dispersed and clumpy in the purely thermal feedback case, and in a more homogeneous ‘shield’ in the simulation including CRs. As discussed in detail in Girichidis et al. (2018) the CRs provide a much smoother outflow leading, for instance, to clumping factors more than one order of magnitude lower than in the ‘noCR’ case (Girichidis et al. 2018, figure 11). In the central panel of Fig. 1, we include an example spectrum where

² Within a given cell, we distribute the starting position uniformly.

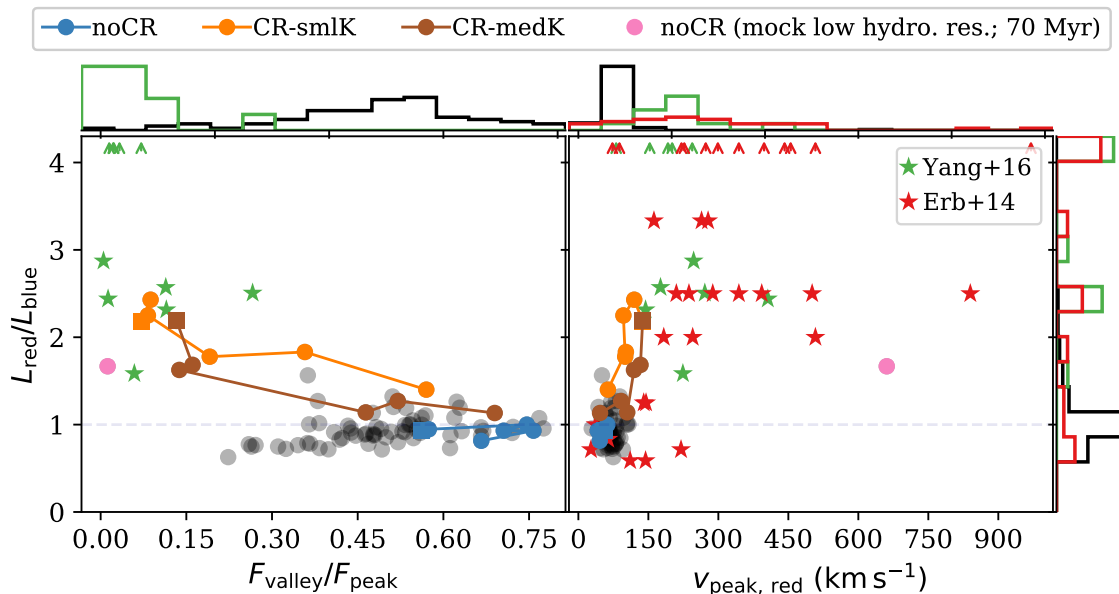


FIG. 3.— Comparison of the modelled Ly α spectra (circles) to observations (stars). We characterize the spectral shape with the asymmetry of the line (y -axis) versus the ‘deepness’ of the draught (*left panel*) and the red peak’s position (*right panel*). In each panel, we highlight our simulated spectra from 40 Myr to 100 Myr by color with the last data point marked with a square. The black circles are other SILCC simulations shown for comparison (see § 3 for details). Note the arrows on the top border of each panel showing the observations with $L_{\text{red}}/L_{\text{blue}} > 4$. In general, only simulations with CRs result in $L_{\text{red}}/L_{\text{blue}}$ and $F_{\text{valley}}/F_{\text{peak}}$ in agreement with observations. The red peak positions are low in all cases.

we cut out the gas at $|z| > 1$ kpc. In that case, when the photons do not have to cross through the CR driven outflow, the spectrum resembles closely the ‘noCR’ case.

To compare our findings to observations, we extract the following characteristics from the computed spectra: (*i*) the ratio of the integrated redward over the integrated blueward flux ($L_{\text{red}}/L_{\text{blue}}$) – which is a measure of the asymmetry of the line shape; (*ii*) the flux at ‘draught’ between the peaks (F_{valley}) in comparison to the flux at the maximum point (F_{peak}), which, in practice, quantifies the ‘deepness’ of the draught of the double peaked spectra; and (*iii*) the position of the red emission peak (v_{red}). We show the evolution of these measures in Fig. 3 from $t = 40$ to 100 Myr (in intervals of 10 Myr) with the last data point marked with a square. We compare this to observations of nearby, star-forming galaxies (the ‘Green Peas’; data taken from Yang et al. 2016, also Henry et al. 2015), and to $z \sim 2 - 3$ Lyman- α selected galaxies (Erb et al. 2014). In addition, we also display other simulation results presented in Walch et al. (2015), Gatto et al. (2017), and Peters et al. (2017) (shown as black circles in Fig. 3). These hydrodynamical simulations include supernovae feedback with random SN positions and cover SN rates from 5 to 45 Myr $^{-1}$ with none including CRs (but partially include stellar wind and UV feedback). We show them only to support the case that the spectral shape we obtain for the ‘noCR’ simulation is not an outlier – but in fact typical for hydrodynamical simulations containing thermal feedback.

Fig. 3 shows that all the simulations without CRs produce Ly α spectra with significant flux at line center ($F_{\text{valley}} \gtrsim 0.4F_{\text{peak}}$; see also the left panel of Fig. 1). This

flux is reduced significantly from $t \gtrsim 30$ Myr in the CR simulations as the outflow is established. Also the asymmetry of the line is increased leading to $L_{\text{red}}/L_{\text{blue}} \sim 2$. Both measures are more in line with what is found in observations where mostly $F_{\text{valley}}/F_{\text{peak}} \lesssim 0.1$ and $L_{\text{red}}/L_{\text{blue}} \gtrsim 2.5$ (see also Steidel et al. 2010; Kulas et al. 2012). Determining F_{valley} observationally requires a high spectral resolution since the convolution of the true spectrum with the instrument’s kernel leads to a spreading of the peak flux, and thus, the true value of F_{valley} can be even lower than measured. This effect makes our comparison of $F_{\text{valley}}/F_{\text{peak}}$ conservative and the true discrepancy between the ‘noCR’ simulation and the observations might be even larger.

In Fig. 3 we illustrate also how the emergent Ly α spectrum changes if the underlying simulation had a lower resolution in the galactic halo which is typically the case for hydrodynamical simulations using adaptive refinement techniques or smoothed particle hydro-dynamics. In order to do this, we used the $t = 70$ Myr snapshot of the ‘noCR’ simulation and averaged the hydrodynamical quantities in blocks of 500 pc sidelength one kiloparsec above and below the disk. The resulting spectral properties (pink circle in Fig. 3) show that the values of $F_{\text{valley}}/F_{\text{peak}}$ and $L_{\text{red}}/L_{\text{blue}}$ are de- and increased compared to the unmodified ‘noCR’ simulation, respectively. We discuss the implications that this purely numerical effect (smoothing due to low resolution) brings the simulated spectra in agreement with observations in Sec. 4.

While the inclusion of CR feedback lowers the tensions between the simulated spectra and the observed asymmetry as well as the flux at line center, this is only par-

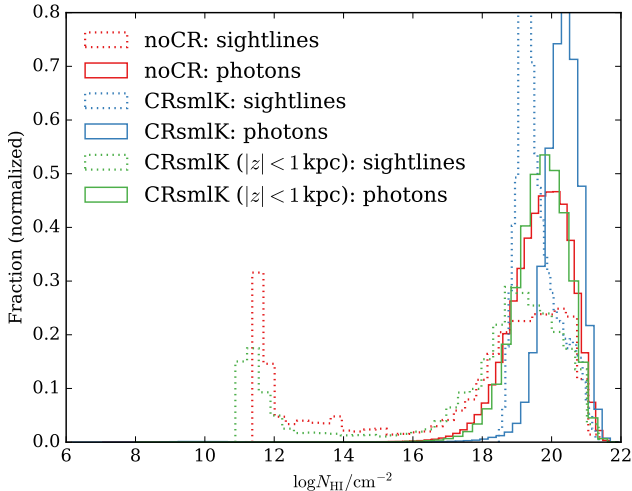


FIG. 4.— Distribution of neutral hydrogen column densities at $t = 70$ Myr. The highly structured outflow (‘noCR’) results in a bimodal column density distribution. For illustration, we also added the distributions for the ‘CRsmlK’ run but with the gas at $|z| > 1$ kpc removed which then resembles closely the ‘noCR’ case.

tially the case for the peak position of the red peak (v_{red} in the right panel of Fig. 3). While CRs seem to increase this measure as well and, thus, bring it close to observed values, the latter can sometimes be as high as $v_{\text{red}} \gtrsim 400 \text{ km s}^{-1}$ which we cannot reproduce (see the following discussion about possible origins of this discrepancy).

4. DISCUSSION & CONCLUSIONS

We have used the hydrodynamical simulations of the star-forming ISM also including magnetic fields and CRs as input for $\text{Ly}\alpha$ radiative transfer calculations and compared computed spectra to observations. Our results show that supernovae, stellar wind, and radiation feedback lead to spectra which are too symmetric and feature too much flux at line center compared to the observations (also Steidel et al. 2010; Kulas et al. 2012). This is caused by low-density channels carved out by the SN feedback, which let $\text{Ly}\alpha$ photons escape at line-center, i.e., without first diffusing in frequency. CRs lead to a ‘shield’ of neutral hydrogen outflowing at $\gtrsim 1$ kpc height, which prevents photons from escaping at line-center.

This is visible from Fig. 4 where we compare for a given time ($t = 70$ Myr) the physical column density distribution (as dotted lines) to the column density crossed by the $\text{Ly}\alpha$ photons (solid lines in Fig. 4). The column density crossed by the $\text{Ly}\alpha$ photons is larger than the physical one due to the scatterings and the resulting increase in pathlength (which leads to a widening of the intrinsic spectrum; cf. Fig. 1). Low-density channels cleared out by supernova feedback leave the physical N_{HI} distribution of the ‘noCR’ simulation bimodal.

Fig. 4 shows also that the photons scatter and diffuse in frequency. This can be seen from the example intrinsic spectrum in Fig. 1 (left, dashed line), which is narrower than the emergent spectrum. Interestingly, this might explain the puzzling fact that the theoretical modelling of observed $\text{Ly}\alpha$ spectra require often a larger ‘intrinsic’ line width than observed through $\text{H}\alpha$ (e.g. Yang et al. 2016; Orlitova et al. 2018). Here, we show that through the turbulence of the inner disk, the line

is widened prior to traversing the wind, yielding wider spectra than the intrinsic one even in the ‘noCR’ case.

The difficulty in reproducing realistic $\text{Ly}\alpha$ spectra from galactic hydrodynamical simulations was noted earlier in the literature (e.g., Gronke et al. 2017). Several other causes for the discrepancy between the simulated $\text{Ly}\alpha$ spectra (without CR feedback) and the observations are possible:

- when comparing to observed $\text{Ly}\alpha$ spectra the partially neutral intergalactic medium might affect the observed $\text{Ly}\alpha$ line shape (Dijkstra et al. 2007). In fact, the effect for $z \gtrsim 3$ is a decrease in flux at line center and a reduction of the blue peak – just as “required”. However, (i) we compare the synthetic $\text{Ly}\alpha$ spectra also to $z \sim 0$ observations where the impact of the IGM on the $\text{Ly}\alpha$ line should be negligible (Laursen et al. 2011); and (ii) even at higher redshift, an absorption of $\sim 50\%$ of the flux of $\text{Ly}\alpha$ emitting galaxies is unlikely because measured values of the $\text{Ly}\alpha$ escape fraction (or EWs) of individual galaxies (e.g., Sobral et al. 2015) as well as the global average of all star-forming galaxies (Hayes et al. 2011; Sobral et al. 2018; Shibuya et al. 2018) suggest higher transmission values.
- the outer circumgalactic medium (CGM) can alter the $\text{Ly}\alpha$ line shape. To assess the importance of this effect a high-resolution ($\sim \text{pc}$) simulation covering a $\sim 10^3 \text{ kpc}^3$ volume is required which would allow to compare modelled $\text{Ly}\alpha$ observables to data. Kakiichi & Dijkstra (2017) showed that observed $\text{Ly}\alpha$ halos surrounding star-forming galaxies (e.g., Wisotzki et al. 2016) can be due to scattered $\text{Ly}\alpha$ radiation without altering the emergent inner $\text{Ly}\alpha$ spectrum heavily. However, more work in this direction is required.
- small-scale, multiphase structure leads $\text{Ly}\alpha$ photons to escape as if the medium is homogeneous, resulting in spectra in agreement with observations (Gronke et al. 2016, 2017). An areal covering fraction of these small ‘droplets’ of unity is required in order for this mechanism to work. This can be due to the in situ production of cold gas (as, e.g., suggested by McCourt et al. 2018), or the uniform transport of it without destruction – which might be achieved through CRs demonstrating that the two proposed mechanisms are not exclusive.

Our setup has limitations (Martizzi et al. 2016) but allowed us to highlight the potentially strong impact of CR driven winds on observed $\text{Ly}\alpha$ spectra. However, our idealized isolated setup ignores larger-scale effects such as filamentary inflows, and differential rotation (Hanasz et al. 2013; Pakmor et al. 2016) on the properties of the cold outflow. Furthermore, the periodic boundary conditions might influence the results slightly. A study using a full galactic disk setup is required to overcome these limitations. It is, however, crucial that this investigation is carried out with sufficient resolution also in the outer regions since – as demonstrated in § 3 – a too low resolution will remove the ionized channels and produce artificially “correct” spectra.

We show that the smooth-uniform outflows generated by CRs leave a clear imprint on the observable Ly α spectrum. For the flux at line center and the asymmetry of Ly α spectra, it is evident that the inclusion of CR feedback brings simulated Ly α spectra more in agreement with observations. Still, the agreement is not perfect: while our models with CRs produce positions of the red peak of $\sim 150 \text{ km s}^{-1}$, this value is lower than the bulk of observations which typically reach $v_{\text{peak,red}} \sim 400 \text{ km s}^{-1}$. This might be due to the solar neighborhood conditions (gas surface densities of $\sim 10 M_{\odot} \text{ pc}^{-2}$), and correspondingly low SN rates of our hydro-dynamical simulations.

Nevertheless, our proposed picture of a cold, neutral CR-driven outflow surrounding the star-forming disk not

only produces naturally the low flux at line center as well as the redward asymmetry of the line but also the widened ‘intrinsic’ Ly α spectra sometimes required. All these points motivate further studies for the impact of CR feedback on Ly α observables.

MG thanks the organizers and participants of ‘SakuraCLAW’, the MPA visitor program, and NASA grant NNX17AK58G. PG acknowledges funding from the ERC under ERC-CoG grant CRAGSMAN-646955. TN and SW acknowledge support by the DFG priority program ‘Physics of the interstellar medium’. SW greatly acknowledges funding by the ERC through the ERC Starting Grant no. 679852 RADFEEDBACK. This research made use of yt (Turk et al. 2011).

REFERENCES

- Cantalupo, S., Porciani, C., & Lilly, S. J. 2008, *ApJ*, 672, 48
Dijkstra, M. 2017, preprint, arXiv:1704.03416
Dijkstra, M., Lidz, A., & Wyithe, J. S. B. 2007, *MNRAS*, 377, 1175
Dubey, A., Reid, L. B., Weide, K., et al. 2009, preprint
Eide, M. B., Gronke, M., Dijkstra, M., & Hayes, M. 2018, *ApJ*, 856, 156
Erb, D. K., Steidel, C. C., Trainor, R. F., et al. 2014, *ApJ*, 795, 33
Fryxell, B., Olson, K., Ricker, P., et al. 2000, *ApJS*, 131, 273
Gatto, A., Walch, S., Low, M.-M. M., et al. 2015, *MNRAS*, 449, 1057
Gatto, A., Walch, S., Naab, T., et al. 2017, *MNRAS*, 466, 1903
Girichidis, P., Naab, T., Hanasz, M., & Walch, S. 2018, preprint, arXiv:1805.09333
Girichidis, P., Naab, T., Walch, S., et al. 2016a, *ApJ*, 816, L19
Girichidis, P., Walch, S., Naab, T., et al. 2016b, *MNRAS*, 456, 3432
Glover, S. C. O., & Clark, P. C. 2012, *MNRAS*, 421, 116
Gronke, M. 2017, *A&A*, 608, A139
Gronke, M., & Dijkstra, M. 2014, *MNRAS*, 1103, 10
Gronke, M., Dijkstra, M., McCourt, M., & Peng Oh, S. 2016, *ApJ*, 833, 1
Gronke, M., Dijkstra, M., McCourt, M., & Peng Oh, S. 2017, *A&A*, 607, A71
Haid, S., Walch, S., Naab, T., et al. 2016, *MNRAS*, 460, 2962
Hanasz, M., Lesch, H., Naab, T., et al. 2013, *ApJ*, 777, L38
Hayes, M., Schaerer, D., Östlin, G., et al. 2011, *ApJ*, 730, 8
Henry, A., Scarlata, C., Martin, C. L., & Erb, D. 2015, *ApJ*, 809, 19
Hui, L., & Gnedin, N. Y. 1997, *MNRAS*, 292, 27
Kakiichi, K., & Dijkstra, M. 2017, preprint, arXiv:1710.10053
Kim, C.-G., & Ostriker, E. C. 2018, *ApJ*, 853, 173
Kulas, K. R., Shapley, A. E., Kollmeier, J. A., et al. 2012, *ApJ*, 745, 33
Laursen, P., Sommer-Larsen, J., & Andersen, A. C. 2009, *ApJ*, 704, 1640
Laursen, P., Sommer-Larsen, J., & Razoumov, A. O. 2011, *ApJ*, 728, 52
Martizzi, D., Fielding, D., Faucher-Giguère, C. A., & Quataert, E. 2016, *MNRAS*, 459, 2311
Mccourt, M., Oh, S. P., O’Leary, R., & Madigan, A.-M. 2018, *MNRAS*, 473, 5407
McKee, C. F., & Ostriker, J. P. 1977, *ApJ*, 218, 148
Naab, T., & Ostriker, J. P. 2017, *ARA&A*, 55, 59
Neufeld, D. A. 1990, *ApJ*, 350, 216
Orlitova, I., Verhamme, A., Henry, A., et al. 2018, ArXiv e-prints, arXiv:1806.01027
Pakmor, R., Pfrommer, C., Simpson, C. M., & Springel, V. 2016, *ApJ*, 824, L30
Partridge, R. B., & Peebles, P. J. E. 1967, *ApJ*, 147, 868
Pei, Y. C. 1992, *ApJ*, 395, 130
Peters, T., Naab, T., Walch, S., et al. 2017, *MNRAS*, 466, 3293
Shibuya, T., Ouchi, M., Konno, A., et al. 2018, *PASJ*, 70, S14
Smith, A., Safranek-Shrader, C., Bromm, V., & Milosavljevi, M. 2015, *MNRAS*, 449, 4336
Sobral, D., Matthee, J., Darvish, B., et al. 2015, *ApJ*, 808, 139
Sobral, D., Santos, S., Matthee, J., et al. 2018, *MNRAS*, 476, 4725
Steidel, C. C., Erb, D. K., Shapley, A. E., et al. 2010, *ApJ*, 717, 289
Tumlinson, J., Peebles, M. S., & Werk, J. K. 2017, *ARA&A*, 55, 389
Turk, M. J., Smith, B. D., Oishi, J. S., et al. 2011, *ApJS*, 192, 9
Veilleux, S., Cecil, G., & Bland-Hawthorn, J. 2005, *ARA&A*, 43, 769
Waagan, K., Federrath, C., & Klingenberg, C. 2011, *Journal of Computational Physics*, 230, 3331
Walch, S., Girichidis, P., Naab, T., et al. 2015, *MNRAS*, 454, 246
Wisotzki, L., Bacon, R., Blaizot, J., et al. 2016, *A&A*, 587, A98
Wünsch, R., Walch, S., Dinmbier, F., & Whitworth, A. 2018, *MNRAS*, 475, 3393
Yang, H., Malhotra, S., Gronke, M., et al. 2016, *ApJ*, 820, 130